SCIENTIFIC REPORTS
nature research

OPEN

Enhancing violations of Leggett-Garg inequalities in nonequilibrium correlated many-body systems by interactions and decoherence

J. J. Mendoza-Arenas[1], F. J. Gómez-Ruiz[2,1*], F. J. Rodríguez[1] & L. Quiroga[1]

We identify different schemes to enhance the violation of Leggett-Garg inequalities in open many-body systems. Considering a nonequilibrium archetypical setup of quantum transport, we show that particle interactions control the direction and amplitude of maximal violation, and that in the strongly-interacting and strongly-driven regime bulk dephasing enhances the violation. Through an analytical study of a minimal model we unravel the basic ingredients to explain this decoherence-enhanced quantumness, illustrating that such an effect emerges in a wide variety of systems.

For several decades, assessing the existence of genuine quantum behavior[1] and quantifying coherence in quantum systems[2] have remained as fundamental open problems, critical to applications in computation and information processing. A seminal breakthrough in this direction was made by Leggett and Garg[3,4], who considered the conditions that a macroscopic system entirely described by classical physics should satisfy. These are macroscopic realism (a system's property is well defined at every time regardless of whether it is observed or not) and noninvasive measurability (the system is unaffected by measurements on it). When these conditions are met, the system satisfies the so-called Leggett-Garg inequalities (LGIs). The experimental observation of their violation, which serves as witness of quantum coherence, has been sought intensively and reported in various platforms[5–9].

In order to establish realistic conditions where LGIs are maximally violated, providing optimal settings for quantum protocols performed in a particular system, its unavoidable coupling to the environment has to be considered. Recent theoretical research on few-qubit systems has determined that Markovian noise degrades quantumness[10–14], while non-Markovianity helps restore it[15–17]. However, many-body interacting systems, where spectacular effects resulting from quantum coherence emerge, remain unexplored within this effort. The non-trivial impact of dissipation in multilevel systems is known to induce unexpected beneficial effects, as entanglement generation and quantum state engineering[18–21], restoration of hidden quantum phase transitions[22] and environment-assisted transport[23–26], recently observed in several quantum simulators[27–30]. Thus such systems constitute attractive candidates for uncovering novel mechanisms of LGI violation enhancement.

In the present work we establish such mechanisms in testbed open many-body systems. We show that not only particle interactions, but also bulk dephasing, can increase the violation of LGIs in Markovian systems. For this we assess the quantumness of the transport supported by interacting spin chains when driven out of equilibrium by unequal boundary reservoirs, a configuration considered so far for LGIs on single-particle systems only[31,32]. Using a minimal model to illustrate the basic ingredients responsible for this phenomenon, we argue that it can emerge under a wide range of conditions.

Methods

Nonequilibrium setup. We consider a spin-1/2 chain coupled to two reservoirs of unequal magnetization at its boundaries, as depicted in Fig. 1. These induce a net homogeneous spin current in its nonequilibrium steady state (NESS)[33–38]. The chain is characterized by the one-dimensional XXZ Hamiltonian

$$\hat{\mathcal{H}} = \tau \sum_{n=1}^{L-1} [\hat{\sigma}_n^x \hat{\sigma}_{n+1}^x + \hat{\sigma}_n^y \hat{\sigma}_{n+1}^y + \Delta \hat{\sigma}_n^z \hat{\sigma}_{n+1}^z], \tag{1}$$

[1]Departamento de Física, Universidad de los Andes, A.A. 4976, Bogotá, D. C., Colombia. [2]Donostia International Physics Center, E-20018, San Sebastián, Spain. *email: fj.gomez34@dipc.org

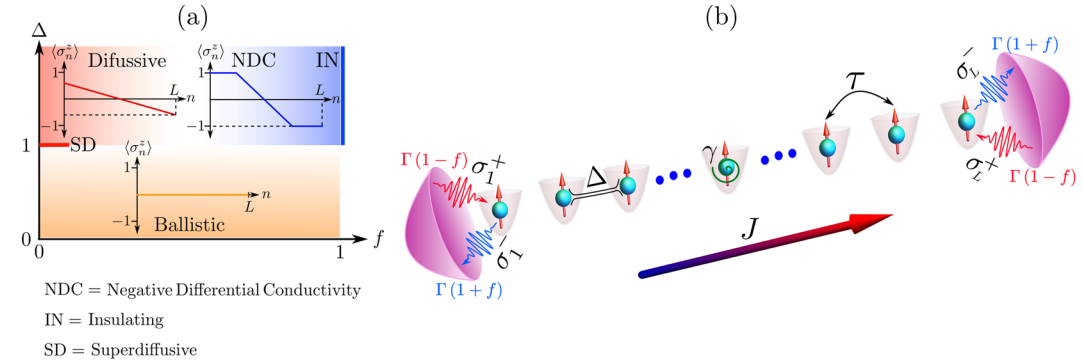

Figure 1. Scheme of the system under study. An XXZ spin chain is coupled to unequal reservoirs at its boundaries, which drive it to a NESS where a spin current J flows from left to right. The nonequilibrium $\Delta - f$ phase diagram is also shown, where characteristic magnetization profiles are depicted for each conduction regime. These correspond to a flat profile for ballistic transport, a ramp with homogeneous slope for diffusion, and ferromagnetic domains for the insulating state.

where $\hat{\sigma}_n^\alpha$ are the Pauli matrices ($\alpha = x, y, z$), L is the number of sites, τ is the exchange interaction (we set the energy scale by taking $\tau = 1$), and Δ is the anisotropy along z direction; we take $\Delta \geq 0$ without loss of generality. When mapping the model to a spinless-fermion description, τ corresponds to the hopping and $\tau\Delta$ to a density-density interaction; thus $\Delta > 1$ is referred to as the strongly-interacting regime.

The boundary reservoirs are modeled as noninteracting spin chains with different average magnetization. In addition, both are weakly coupled to the XXZ chain, and their time correlations decay very rapidly, so their memory effects can be neglected (Markov approximation). Furthermore, the so-called wide-band limit is considered, where the bandwidths of the reservoirs, proportional to their hopping rates, are much larger than the bandwidth of the XXZ chain. Invoking these assumptions[34,39], and following standard microscopic derivations where the degrees of freedom of the reservoirs are traced out[40], it is shown that the dynamics of the chain under the influence of the environment is governed by a Lindblad master equation,

$$\dot{\hat{\rho}}_t = \hat{\mathcal{L}}(\hat{\rho}) = -i[\hat{\mathcal{H}}, \hat{\rho}] + \sum_k \hat{V}_k \hat{\rho} \hat{V}_k^\dagger - \frac{1}{2}\{\hat{V}_k^\dagger \hat{V}_k, \hat{\rho}\}. \tag{2}$$

Here $\hat{\rho}$ is the density matrix of the chain, $\hat{\mathcal{L}}$ is the Lindblad superoperator, {.,.} is the anticommutator of two operators, and $\hat{V}_k$ correspond to the jump operators establishing the coupling of the chain to the environment. For the boundary driving we consider operators that annihilate ($\hat{V}^-$) and create ($\hat{V}^+$) spin excitations at both the left (ℓ) and right (r) edges of the chain, given by $\hat{V}_{r,\ell}^- = \sqrt{\Gamma(1 \mp f)}\,\hat{\sigma}_{1,L}^-$ and $\hat{V}_{r,\ell}^+ = \sqrt{\Gamma(1 \pm f)}\,\hat{\sigma}_{1,L}^+$. Here Γ is the coupling strength (we take $\Gamma = 1$), and $\pm f$ are the average magnetizations per spin (in dimensionless units[34]) of the left/right reservoirs. Thus the parameter f ($0 \leq f \leq 1$) is the driving, as it establishes the magnetization imbalance between the boundaries. If $f = 0$, spin excitations are created and annihilated at the same rate on both boundaries, so there is no net magnetization imbalance and thus no spin transport. If $f > 0$, more excitations are created (annihilated) on the left-most (right-most) site of the lattice, inducing a net current resulting from a left-to-right flow and its weaker backflow. We also consider bulk dephasing processes, arising from the coupling of every site of the XXZ chain to local harmonic vibrational degrees of freedom corresponding to the oscillation of the lattice, and quantized in terms of linear phonons[39]. Tracing out these degrees of freedom, and considering the wide-band limit, the resulting jump operators are $\hat{V}_n^z = \sqrt{\gamma}\,\hat{\sigma}_n^z$ ($n = 1, \ldots, L$), where γ is the homogeneous dephasing rate.

When the spin chain evolves in time as dictated by Eq. (2), it eventually reaches its unique NESS, given by $\hat{\rho}_\infty = \lim_{t\to\infty} \hat{\rho}(t) = \lim_{t\to\infty} \exp[\hat{\mathcal{L}}(t)]\hat{\rho}(0)$, with $\hat{\rho}(0)$ an initial state. Its transport properties are characterized by its magnetization profile $\langle \hat{\sigma}_n^z \rangle$ and the homogeneous spin current $J = \langle \hat{\mathrm{J}}_n \rangle$, with $\hat{\mathrm{J}}_n = 2(\hat{\sigma}_n^x \hat{\sigma}_{n+1}^y - \hat{\sigma}_n^y \hat{\sigma}_{n+1}^x)$. The phase diagram of the dephasing-free model, obtained from the behavior of both quantities, is depicted in Fig. 1. For weak driving f (linear response), $\Delta < 1$ shows ballistic conduction while for $\Delta > 1$ the system satisfies a normal diffusion equation[33,34]. This indicates a nonequilibrium quantum phase transition at the isotropic point $\Delta = 1$, which is super-diffusive[41]. For large driving f and $\Delta > 1$, negative differential conductivity (NDC) emerges, leading to an insulting state at maximal driving $f = 1$ in which opposite-polarized ferromagnetic domains suppress transport[34–36]. This behavior is absent at $\Delta < 1$, where transport remains ballistic for any f.

In the presence of dephasing, spin transport is monotonically degraded with γ and becomes diffusive for $\Delta < 1$[42], while it is largely enhanced with γ for $\Delta > 1$, a manifestation of strong correlations[35]. The enhancement vastly increases with driving, as dephasing washes out the NDC and induces an insulator-conducting transition at $f = 1$.

Results

Leggett-garg inequalities calculation. As shown by Leggett and Garg[3,4], macroscopic classical systems satisfy the inequaity $\mathcal{C}(t_1, t_2) + \mathcal{C}(t_2, t_3) - \mathcal{C}(t_1, t_3) \leq 1$ ($t_1 < t_2 < t_3$). Here $\mathcal{C}(t_i, t_j)$ denotes the two-time correlations of a dichotomic operator $\hat{Q}$ (with eigenvalues ± 1) between times t_i and t_j, and is given by $\mathcal{C}(t_i, t_j) = \frac{1}{2}\langle\{\hat{Q}(t_i), \hat{Q}(t_j)\}\rangle$. For the NESS $\hat{\rho}_\infty$, which is unaffected by an evolution under $\hat{\mathcal{L}}$, this correlation with $t_i < t_j$ is given by

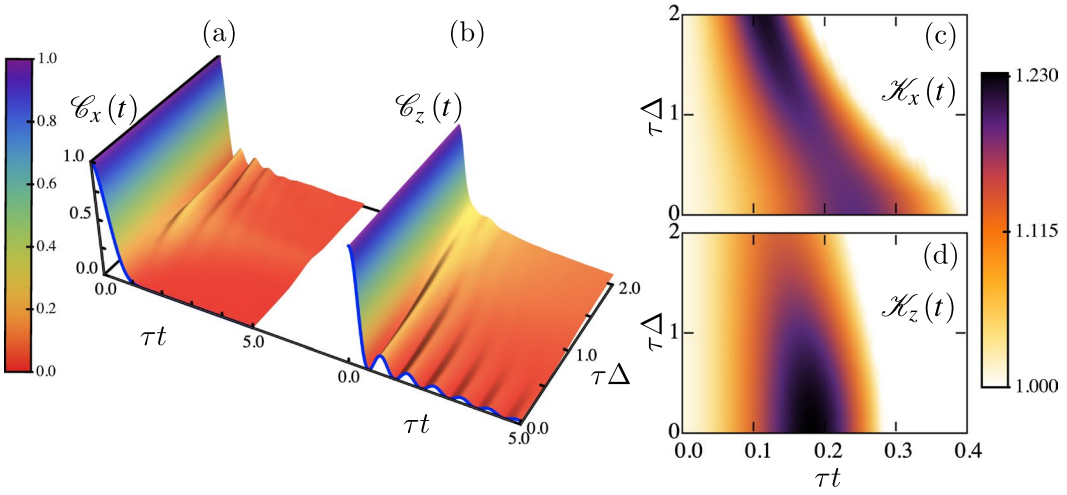

Figure 2. Time correlations $\mathcal{C}_\alpha(t)$ (**a**,**b**) and Leggett-Garg functions $\mathcal{K}^\alpha(t)$ (**c**,**d**) as a function of time and anisotropy Δ for weak driving $f=0.1$ and system size $L=60$. (**a**,**c**) $\alpha=x$. (**b**,**d**) $\alpha=z$. The blue lines in (**a**,**b**) are the infinite-temperature correlations described in the main text for $\Delta=0$. In (**c**,**d**) the LGI is violated (satisfied) in the colored (white) regions.

$$\mathcal{C}(t_i, t_j) = \mathrm{Re}\,(\mathrm{Tr}\,[\hat{Q}\exp[\hat{\mathcal{L}}(t_j - t_i)]\hat{Q}\hat{\rho}_\infty]). \tag{3}$$

Thus, $\mathcal{C}(t_i, t_j) = \mathcal{C}(0, t_j - t_i)$, and taking time intervals $t_2 - t_1 = t_3 - t_2 = t$, the LGI reduces to $\mathcal{K}(t) \equiv 2\mathcal{C}(t) - \mathcal{C}(2t) \leq 1$, where we define the Leggett-Garg function $\mathcal{K}(t)$, and $\mathcal{C}(t) \equiv \mathcal{C}(0, t)$. Note that we cannot regard the nature of transport as classical from observing that the LGI for some $\hat{Q}$ is satisfied, as it might not capture the quantum correlations that inequalities for other measurements might. However, we do assess genuine quantum behavior when one LGI is violated[31].

We focus on LGIs when performing measurements of local observables $\hat{Q} = \hat{\sigma}_l^\alpha$ ($\alpha=x, z$) for site $l=L/2$ on the NESS $\hat{\rho}_\infty$. In this form we reduce edge effects as much as possible; however we have verified that the results are qualitatively the same when performing the measurements on different sites (see Fig. S2 of the Supplementary Information (SI) (See Supplementary Information). To evaluate the LGIs violation in the boundary-driven setup for large systems, we obtain their NESS applying the time-dependent density matrix renormalization group[43,44], describing the state by a matrix product structure[33,45]. Then we calculate the time evolution of Eq. (3) to obtain the single-site two-time correlations, from which the Leggett-Garg function $\mathcal{K}(t)$ follows immediately. Our simulations are based on the open-source Tensor Network Theory (TNT) library[46,47]. This constitutes a novel and topical application of matrix product states, fueled by the growing interest in evaluating two-time correlations in dissipative many-body systems[48–52].

Controlling LGI violations with interactions: dephasing free case. We now show that violations of LGIs can be tuned by interactions, and can indicate nonequilibrium quantum phase transitions. For this we consider the linear-response regime, where the system presents a transition from ballistic ($\Delta<1$) to diffusive ($\Delta>1$) spin transport. In Fig. 2(a,b) we show $\mathcal{C}_\alpha(t)$ for $\alpha=x, z$, which measure the response of the system when adding or removing a spin excitation for $\alpha=x$, or measuring the local magnetization for $\alpha=z$. These correlations already show a qualitative difference, most notable for early times, between the two transport regimes. First, since for $\Delta=0$ and weak driving the NESS is very close to an identity[53,54] (with terms of $\mathcal{O}(f)$ accounting for the spin current and magnetization and higher-order corrections for correlations), the results are very well approximated by known analytical results for an infinite-temperature state. These correspond to an exponential decay[55] for $\alpha=x, \mathcal{C}_x(t) \approx e^{-4\tau^2t^2}$, and a squared Bessel function[56] for $\alpha=z, \mathcal{C}_z(t) \approx \mathcal{J}_0^2(4\tau t)$, thus being independent of the details of the driving. The qualitative behavior continues when increasing Δ approximately till the isotropic point. For the strongly interacting regime, the correlations $\mathcal{C}_x(t)$ develop early oscillations of frequency $\sim\Delta^{-1}$, while those of $\mathcal{C}_z(t)$ are strongly suppressed.

In Fig. 2(c,d) we show the corresponding Leggett-Garg functions; these are obtained exactly for $\Delta=0$, namely $\mathcal{K}^x(t) = 2e^{-4\tau^2t^2} - e^{-16\tau^2t^2}$ and $\mathcal{K}^z(t) = 2\mathcal{J}_0^2(4\tau t) - \mathcal{J}_0^2(8\tau t)$, which agree with our numerical simulations. For all Δ and early times the inequalities in both directions are violated, indicating genuine quantum behavior which cannot be accounted for by a classical description[a]. In Fig. 3 we show the maximal violations $\mathcal{K}^\alpha_{\mathrm{Max}}$ as a function of Δ, and observe that while the function of $\alpha=z$ monotonically decreases with interactions, that of $\alpha=x$ has a non-monotonic behavior, but increases for $\Delta>1$. Moreover, at the isotropic point the direction along which the LGI violation becomes maximal changes, from $\alpha=z$ for $\Delta<1$ to $\alpha=x$ for $\Delta>1$. As a result, the direction and magnitude of the overall maximal violation can be controlled by Δ, being enhanced in the strongly-interacting regime.

[a]We do not consider longer times, where revivals of the LGI violations occur, as we are mostly interested in the maximal violations $\mathcal{K}^\alpha_{\mathrm{Max}}$, which take place at an early time.

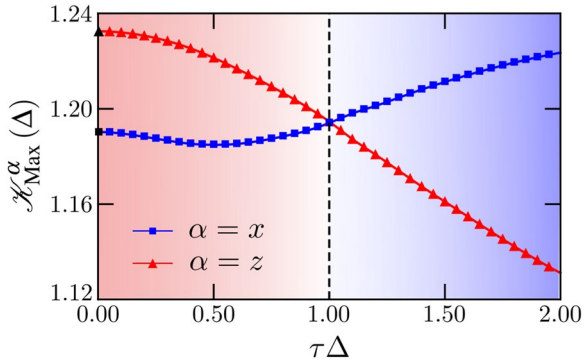

Figure 3. Maximum violation of LGI along x and z directions as a function of anisotropy Δ, for weak driving $f=0.1$ and size $L=60$. The black filled symbols at $\Delta=0$ correspond to the infinite-temperature results described in the main text.

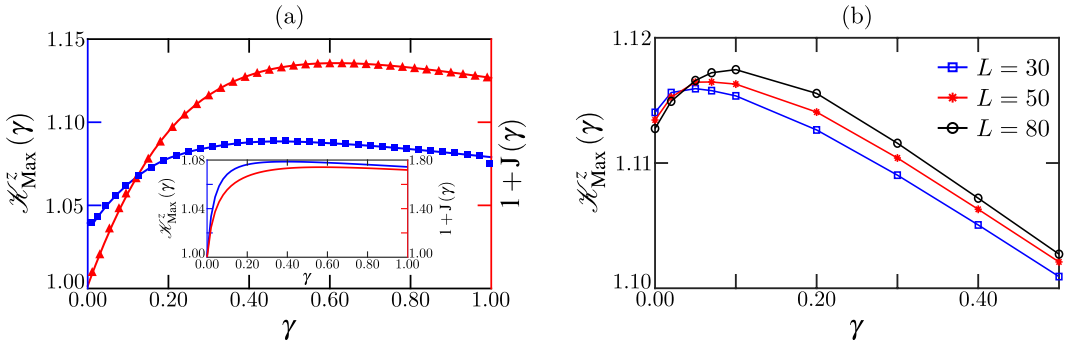

Figure 4. (**a**) Maximum violation of LGI for the XXZ chain along z direction (blue solid line, squares) and shifted spin current (red dashed line, triangles) as a function of dephasing γ for $L=16$, anisotropy $\Delta=2$ and driving $f=1$. Inset: Maximal violation (blue solid line) and current (red dashed line) for the minimal model with $f=1$, $K=10$, $\delta=1$ and $\Gamma=1$. (**b**) Dephasing-enhanced LGI violation at intermediate driving. We depict the maximal LGI violation for $\alpha=z$ as a function of dephasing rate γ, for $\Delta=2$, $f=0.5$ and different system sizes L.

This also shows that the LGI violation indicates the nonequilibrium critical point, a property that it also features in equilibrium[57,58].

Dephasing-enhanced LGI violations. Now we discuss LGIs of the driven system in the presence of bulk dephasing. As previously mentioned, for strong interactions $\Delta>1$ and large driving $f=1$ dephasing melts the ferromagnetic domains that suppress transport, inducing a transition to a conducting state. Thus the spin current is enhanced with γ by several orders of magnitude, as shown in Fig. 4(a). This constitutes a many-body scheme of environment-assisted transport[35]. Here we calculate the maximum violation of the LGI for $\alpha=z$ as a function of γ, also shown in Fig. 4(a). Small systems are considered to be able to calculate the NESS in the absence of (or for very weak) dephasing, which takes an exponentially-long time due to the presence of the ferromagnetic domains[34,35].

For $\gamma=0$ LGIs are markedly violated, since operator $\hat{Q}$ is applied between the ferromagnetic domains and induces appreciable dynamics. But remarkably, as the system becomes conducting due to weak dephasing, it also presents enhanced quantumness measure manifested in the increase of the violations. Even for stronger dephasing $\gamma\approx 1$, where $\mathcal{K}^{z}_{\rm Max}$ decreases with γ, the violation is still larger than that of $\gamma=0$. Thus there is a wide range of environmental couplings where in addition to a large transport enhancement, quantum features are strengthened. This is in stark contrast to the weakly-interacting case, depicted in Fig. S1 of the SI (See Supplementary Information), where both the spin transport and the violation of LGIs are monotonically degraded with dephasing. This indicates that the origin of the observed effect is truly a consequence of strong interactions between particles, a scenario where LGIs remain largely unexplored.

We also observe enhanced violation of LGIs with dephasing even for much weaker driving f, where for $\gamma=0$ the system is conducting and the differential conductivity is positive (as NDC emerges at larger driving)[34,35]. In Fig. 4(b) we present the maximal violation as a function of γ for $\Delta=2$ and an intermediate driving $f=0.5$, in which the system is conducting and far away from the insulating limit. We first note that in the absence of dephasing, the violation for $f=0.5$ is larger than that at $f=1$ (see Fig. 4(a)), which shows that just making the system conducting by inducing a magnetization backflow increases the quantumness measure in the lattice. Furthermore,

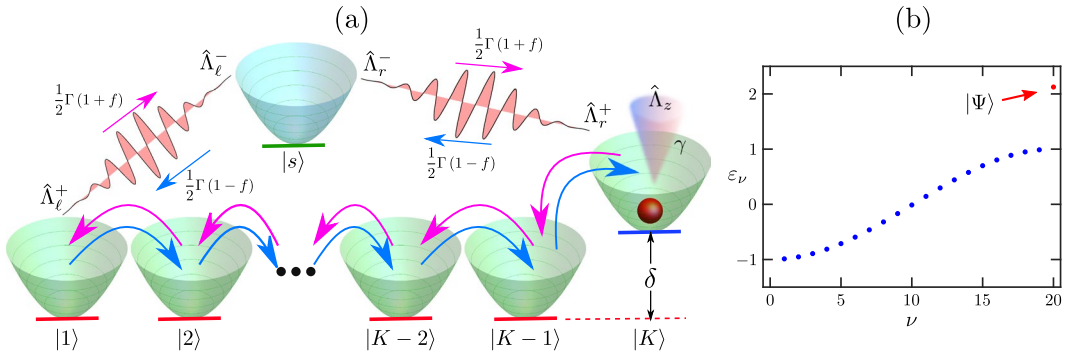

Figure 5. Minimal model. (**a**) Schematic illustration. A single-particle system is incoherently coupled to an auxiliary state $|s\rangle$, which induces a current with driving f. (**b**) Eigenstructure. The depicted energies ε_ν correspond to $K=20$ and $\delta=2$. The gap between the most energetic eigenstate $|\Psi\rangle$ (red dot), preferentially populated at maximal driving and zero dephasing (see Eq. (S1) of the SI), and the conducting band, is of $\mathcal{O}(\delta)$.

when dephasing is included, it increases the violation compared to the $\gamma=0$ case; this indicates that the effect is not just a peculiarity of the maximally-driven limit, but emerges in a broader transport regime. The key ingredient is again the existence of strong interactions Δ. This strongly contrasts with the natural expectation that in conducting regimes, environmental coupling degrades LGI violations[31,59].

It is important to stress two additional properties evidenced in Fig. 4(b). First, the maximal violation barely changes with the system size, indicating that this is not a small-lattice effect. We have performed simulations around the optimal dephasing rate for systems of up to $L=150$, and observed that $\mathcal{K}^z_{\rm Max}$ slightly increases with L, from $\mathcal{K}^z_{\rm Max}=1.116$ for $L=30$ to $\mathcal{K}^z_{\rm Max}=1.120$ (not shown). Thus for large systems the positive impact of dephasing is still present and of almost the same amplitude of that at much smaller lattices. Second, the optimal dephasing slightly shifts to higher values with L, but for the largest chains considered, it remains $\approx$0.10. This leads to a wide range of dephasing rates for which the LGI violation is larger than that of the $\gamma=0$ limit.

Finally, we note that the LGI violation enhancement by dephasing is also observed when non-local observables $\hat{Q}$ are considered. In particular, we calculated the two-time correlations for strings of operators $\hat{Q}=\hat{\sigma}^z_l\hat{\sigma}^z_{l+1}\hat{\sigma}^z_{l+2}\cdots\hat{\sigma}^z_n$ of different length, located around the center of the XXZ lattice. The results, shown of Fig. S3 of the SI (See Supplementary Information), are very similar to those of Fig. 4, both at and away from strong driving, where the maximal LGI violation takes place at a finite dephasing rate. This makes our conclusions more robust, and suggests that this phenomenon could be observed in experiments where measurements are performed on a non-local basis.

Minimal model. To obtain more insight into the incoherent enhancement of LGI violations, we analyze a simple model which incorporates the essential ingredients of the strongly-interacting lattice[35]. This model, depicted in Fig. 5, mimics its gapped eigenstructure, consisting of flat (insulating) and wide (conducting) bands, and the population transfer between them due to coherent processes, incoherent driving and dephasing. It consists of K levels $|1\rangle$, …, $|K\rangle$, with Hamiltonian

$$\hat{\mathcal{H}}_{\rm Min}=\frac{1}{2}\sum_{k=1}^{K-1}\left(|k\rangle\langle k+1|+\text{H.c.}\right)+\delta|K\rangle\langle K|, \tag{4}$$

where state $|K\rangle$ is elevated in energy with respect to the others by an amount $\delta>0$; thus the bands are separated by a gap of $\mathcal{O}(\delta)$, similarly to the strongly-interacting XXZ model (gaps of $\mathcal{O}(\Delta)$). The driving is modeled by the incoherent coupling of states $|1\rangle$ and $|K\rangle$ to an auxiliary site $|s\rangle$, with jump operators $\hat{V}^-_{\ell,r}=\sqrt{\Gamma(1\mp f)}\,\hat{\Lambda}^-_{\ell,r}$ and $\hat{V}^+_{\ell,r}=\sqrt{\Gamma(1\pm f)}\,\hat{\Lambda}^+_{\ell,r}$, where $\hat{\Lambda}^-_\ell=|s\rangle\langle 1|$, $\hat{\Lambda}^+_r=|K\rangle\langle s|$, $\hat{\Lambda}^+_\ell=(\hat{\Lambda}^-_\ell)^\dagger$ and $\hat{\Lambda}^-_r=(\hat{\Lambda}^+_r)^\dagger$. In addition, the dephasing at rate γ corresponds to the jump operator $\hat{\Lambda}_z=\sqrt{\gamma}(\hat{I}-2|K\rangle\langle K|)$, with identity $\hat{I}$, which is equivalent to $\hat{\sigma}^z$ in the XXZ model and acts only on the state of highest energy. This is similar to the effect of dephasing on the original many-body system, which induces transitions from high-energy flat bands of the eigenstructure to low-energy wide bands of higher conduction[35]. Finally, the associated local current operator is $\hat{\mathcal{J}}_{{\rm Min},k}=-i(|k\rangle\langle k+1|-\text{H.c.})$.

This model leads to the emergence of NCD, an insulating state at $f=1$ and dephasing-enhanced transport. These effects are shown in Fig. 6(a) for $K=10$, $\Gamma=1$ and $\delta=1$. Note that $\delta=1$ does not correspond to the isotropic point of the XXZ model. The model does not capture the transport phase transition, as it is defined to mimic the strongly-interacting regime of the spin chain. Here δ sets the size of the gap between bands[35]. We clearly see that when $\gamma=0$ the system is insulating at maximal driving $f=1$, where the equivalent of the ferromagnetic domains is a preferred population of state $|K\rangle$ (see Eq. (S1) of the SI). The NDC is washed out by dephasing, which results in a large transport enhancement with γ. For large dephasing the transport is degraded, as a result of the Zeno effect which tends to freeze the dynamics. Thus the main transport properties of the strongly-interacting XXZ system are captured by the minimal model.

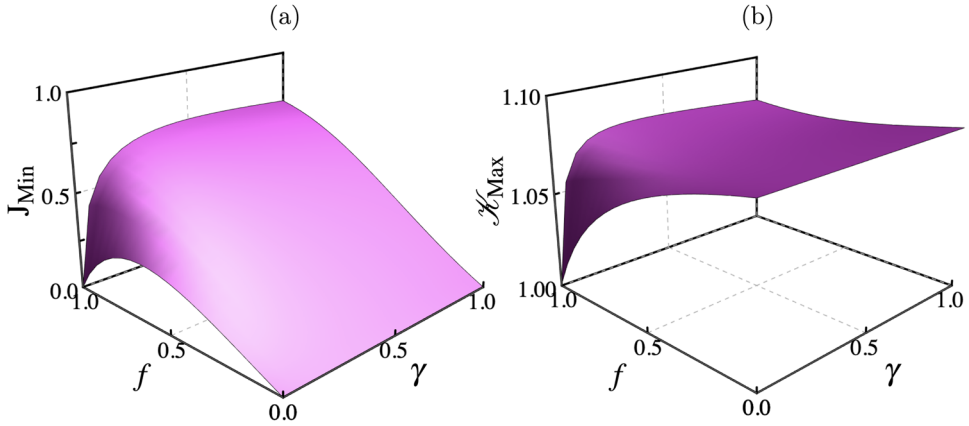

Figure 6. Physical properties of the minimal model. (**a**) Current $J_{Min} = \langle \hat{J}_{Min,k} \rangle$ as a function of driving f and dephasing γ. (**b**) Corresponding maximal value of the Leggett-Garg function, i.e. maximal violation of LGI.

To study LGIs, we calculate the time correlations for the operator $\hat{Q} = \hat{\mathcal{I}} - 2|P\rangle\langle P|$, where site P is taken on the central site of the system. Exact numerical results of the Leggett-Garg function $\mathcal{K}(t)$ are depicted in Fig. 6(b), showing that, similarly to the original model, two mechanisms enhance the violations of LGIs with respect to the dephasing-free $f=1$ limit (where there is no visible violation), namely introducing a backflow ($f<1$) or dephasing ($\gamma>0$). Very large dephasing degrades this scenario, as expected. Thus in spite of its simplicity, the model features the essential ingredients underlying such phenomena.

Analytical results up to $\mathcal{O}(\delta^{-2})$ for the strongly-driven limit, where the effects of decoherence are the largest, help determine how LGI violations are increased; see details in the SI (See Supplementary Information). For the dephasing-free system with $f=1$, $\mathcal{C}^{(0)}(t) \approx \mathcal{K}^{(0)}(t) \approx 1$, so the LGI is not significantly violated, as expected. Defining $\beta = 2(1-f)(1+\Gamma^2)$ when slightly moving from maximal driving with $\gamma=0$, or $\beta = 16\gamma(1+\Gamma^2)/\Gamma$ when introducing weak dephasing at $f=1$, or their sum if both are present, we get the general behavior

$$\mathcal{K}(t) = 1 + \beta\left(\frac{t}{2\delta}\right)^2. \tag{5}$$

This shows that both mechanisms induce an appreciable violation of the LGI which grows quadratically at early times, and which increases linearly as $(1-f)$ and/or γ. It also manifests that the source of these results, also present in the strongly-interacting XXZ model, is the gapped eigenstructure of the model.

Discussion

We have discussed schemes for increasing violations of Leggett-Garg inequalities in open many-body systems, illustrated in archetypical nonequilibrium boundary-driven configurations. Using matrix product state simulations, we have determined that in the strongly-interacting regime, interactions and (unexpectedly) bulk dephasing can enhance the violations. The main mechanism behind the latter effect is illustrated by the same observation in a minimal model, which mimics the gapped eigenstructure of the original system. Given the simplicity of the studied models, our results pave the way for novel experimental protocols of detecting macroscopic quantum coherence in a large variety of scenarios, including single-particle and many-body inhomogeneous (e.g. disordered[37,38]) current-carrying systems.

Received: 21 August 2019; Accepted: 22 October 2019;
Published online: 28 November 2019

References

1. de Chiara, G. & Sanpera, A. Genuine quantum correlations in quantum many-body systems: a review of recent progress. *Rep. Prog. Phys.* **81**, 074002, https://doi.org/10.1088/1361-6633/aabf61 (2018).
2. Streltsov, A., Adesso, G. & Plenio, M. B. Colloquium: Quantum coherence as a resource. *Rev. Mod. Phys.* **89**, 041003, https://doi.org/10.1103/RevModPhys.89.041003 (2017).
3. Leggett, A. J. & Garg, A. Quantum mechanics versus macroscopic realism: Is the flux there when nobody looks? *Phys. Rev. Lett.* **54**, 857–860, https://doi.org/10.1103/PhysRevLett.54.857 (1985).
4. Emary, C., Lambert, N. & Nori, F. Leggett-Garg inequalities. *Reports on Prog. Phys.* **77**, 016001, https://doi.org/10.1088/0034-4885/77/1/016001 (2014).
5. Palacios-Laloy, A. *et al.* Experimental violation of a Bell's inequality in time with weak measurement. *Nat. Phys.* **6**, 442, https://doi.org/10.1038/nphys1641 (2010).
6. Goggin, M. E. *et al.* Violation of the Leggett-Garg inequality with weak measurements of photons. *Proc. Natl. Acad. Sci.* **108**, 1256–1261, https://doi.org/10.1073/pnas.1005774108 (2011).
7. Knee, G. C. *et al.* Violation of a Leggett-Garg inequality with ideal non-invasive measurements. *Nat. Comms.* **3**, 606, https://doi.org/10.1038/ncomms1614 (2012).
8. Dressel, J., Broadbent, C. J., Howell, J. C. & Jordan, A. N. Experimental Violation of Two-Party Leggett-Garg Inequalities with Semiweak Measurements. *Phys. Rev. Lett.* **106**, 040402, https://doi.org/10.1103/PhysRevLett.106.040402 (2011).

9. Zhou, Z.-Q., Huelga, S. F., Li, C.-F. & Guo, G.-C. Experimental Detection of Quantum Coherent Evolution through the Violation of Leggett-Garg-Type Inequalities. *Phys. Rev. Lett.* **115**, 113002, https://doi.org/10.1103/PhysRevLett.115.113002 (2015).
10. Emary, C. Decoherence and maximal violations of the Leggett-Garg inequality. *Phys. Rev. A* **87**, 032106, https://doi.org/10.1103/PhysRevA.87.032106 (2013).
11. Lobejko, M., Luczka, J. & Dajka, J. Leggett-Garg inequality for qubits coupled to thermal environment. *Phys. Rev. A* **91**, 042113, https://doi.org/10.1103/PhysRevA.91.042113 (2015).
12. Friedenberger, A. & Lutz, E. Assessing the quantumness of a damped two-level system. *Phys. Rev. A* **95**, 022101, https://doi.org/10.1103/PhysRevA.95.022101 (2017).
13. Chanda, T., Das, T., Mal, S., Sen(De), A. & Sen, U. Canonical Leggett-Garg inequality: Nonclassicality of temporal quantum correlations under energy constraint. *Phys. Rev. A* **98**, 022138, https://doi.org/10.1103/PhysRevA.98.022138 (2018).
14. Ban, M. Two-time correlation functions of a two-level system influenced by a composite environment. *Quantum Inf. Process.* **17**, 317, https://doi.org/10.1007/s11128-018-2093-5 (2018).
15. Chen, P.-W. & Ali, M. Investigating Leggett-Garg inequality for a two level system under decoherence in a non-Markovian dephasing environment. *Sci. Rep.* **4**, 6165, https://doi.org/10.1038/srep02514 (2014).
16. Naikoo, J., Banerjee, S. & Srikanth, R. Leggett-Garg inequality violation under non-Markovian noise. Preprint at, https://arxiv.org/abs/1806.00537v1 (2018).
17. Datta, S., Mal, S. & Majumdar, A. Protecting temporal correlations of two-qubit states using quantum channels with memory. Preprint at, https://arxiv.org/abs/1808.10345v1 (2018).
18. Diehl, S. *et al*. Quantum states and phases in driven open quantum systems with cold atoms. *Nat. Phys.* **4**, 878, https://doi.org/10.1038/nphys1073 (2008).
19. Verstraete, F., Wolf, M. M. & Cirac, J. I. Quantum computation and quantum-state engineering driven by dissipation. *Nat. Phys.* **5**, 633, https://doi.org/10.1038/nphys1342 (2009).
20. Lin, Y. *et al*. Dissipative production of a maximally entangled steady state of two quantum bits. *Nature* **504**, 415, https://doi.org/10.1038/nature12801 (2013).
21. Kienzler, D. *et al*. Quantum harmonic oscillator state synthesis by reservoir engineering. *Science* **347**, 53, https://doi.org/10.1126/science.1261033 (2015).
22. Zhang, G., Novais, E. & Baranger, H. U. Rescuing a quantum phase transition with quantum noise. *Phys. Rev. Lett.* **118**, 050402, https://doi.org/10.1103/PhysRevLett.118.050402 (2017).
23. Plenio, M. B. & Huelga, S. F. Dephasing-assisted transport: quantum networks and biomolecules. *New J. Phys.* **10**, 113019, https://doi.org/10.1088/1367-2630/10/11/113019 (2008).
24. Mohseni, M., Rebentrost, P., Lloyd, S. & Aspuru-Guzik, A. Environment-assisted quantum walks in photosynthetic energy transfer. *J. Chem. Phys.* **129**, 174106, https://doi.org/10.1063/1.3002335 (2008).
25. Chin, A. W., Datta, A., Caruso, F., Huelga, S. F. & Plenio, M. B. Noise-assisted energy transfer in quantum networks and light-harvesting complexes. *New. J. Phys.* **12**, 065002, https://doi.org/10.1088/1367-2630/12/6/065002 (2010).
26. Sinayskiy, I., Marais, A., Petruccione, F. & Ekert, A. Decoherence-assisted transport in a dimer system. *Phys. Rev. Lett.* **108**, 020602, https://doi.org/10.1103/PhysRevLett.108.020602 (2012).
27. Viciani, S., Lima, M., Bellini, M. & Caruso, F. Observation of Noise-Assisted Transport in an All-Optical Cavity-Based Network. *Phys. Rev. Lett.* **115**, 083601, https://doi.org/10.1103/PhysRevLett.115.083601 (2015).
28. Gorman, D. J. *et al*. Engineering Vibrationally Assisted Energy Transfer in a Trapped-Ion Quantum Simulator. *Phys. Rev. X* **8**, 011038, https://doi.org/10.1103/PhysRevX.8.011038 (2018).
29. Potočnik, A. *et al*. Studying light-harvesting models with superconducting circuits. *Nat. Commun.* **9**, 904, https://doi.org/10.1038/s41467-018-03312-x (2018).
30. Maier, C. *et al*. Environment-Assisted Quantum Transport in a 10-qubit Network. *Phys. Rev. Lett.* **122**, 050501, https://doi.org/10.1103/PhysRevLett.122.050501 (2019).
31. Lambert, N., Emary, C., Chen, Y.-N. & Nori, F. Distinguishing Quantum and Classical Transport through Nanostructures. *Phys. Rev. Lett.* **105**, 176801, https://doi.org/10.1103/PhysRevLett.105.176801 (2010).
32. Castillo, J. C., Rodríguez, F. J. & Quiroga, L. Enhanced violation of a Leggett-Garg inequality under nonequilibrium thermal conditions. *Phys. Rev. A* **88**, 022104, https://doi.org/10.1103/PhysRevA.88.022104 (2013).
33. Prosen, T. & Žnidarič, M. Matrix product simulations of non-equilibrium steady states of quantum spin chains. *J. Stat. Mech.* P02035, https://doi.org/10.1088/1742-5468/2009/02/P02035 (2009).
34. Benenti, G., Casati, G., Prosen, T., Rossini, D. & Žnidarič, M. Charge and spin transport in strongly correlated onedimensional quantum systems driven far from equilibrium. *Phys. Rev. B* **80**, 35110, https://doi.org/10.1103/PhysRevB.80.035110 (2009).
35. Mendoza-Arenas, J. J., Grujic, T., Jaksch, D. & Clark, S. R. Dephasing enhanced transport in nonequilibrium strongly correlated quantum systems. *Phys. Rev. B* **87**, 235130, https://doi.org/10.1103/PhysRevB.87.235130 (2013).
36. Mendoza-Arenas, J. J., Al-Assam, S., Clark, S. R. & Jaksch, D. Heat transport in an *XXZ* spin chain: from ballistic to diffusive regimes and dephasing enhancement. *J. Stat. Mech. Theor. Exp.* **2013**, P07007, https://doi.org/10.1088/1742-5468/2013/07/P07007 (2013).
37. Žnidarič, M., Scardicchio, A. & Varma, V. K. Diffusive and subdiffusive spin transport in the ergodic phase of a many-body localizable system. *Phys. Rev. Lett.* **117**, 040601, https://doi.org/10.1103/PhysRevLett.117.040601 (2016).
38. Žnidarič, M., Mendoza-Arenas, J. J., Clark, S. R. & Goold, J. Dephasing enhanced spin transport in the ergodic phase of a many-body localizable system. *Annalen der Physik* **529**, 1600298, https://doi.org/10.1002/andp.201600298 (2017).
39. Mendoza-Arenas, J. J. *Spin and energy transport in boundary-driven low-dimensional open quantum systems*. Ph.D. thesis, University of Oxford (2014).
40. Breuer, H.-P. & Petruccione, F. *The theory of open quantum systems* (Oxford University Press, Oxford, 2002).
41. Žnidarič, M. Spin Transport in a One-Dimensional Anisotropic Heisenberg Model. *Phys. Rev. Lett.* **106**, 220601, https://doi.org/10.1103/PhysRevLett.106.220601 (2011).
42. Žnidarič, M. Dephasing-induced diffusive transport in anisotropic Heisenberg model. *New J. Phys.* **12**, 043001, https://doi.org/10.1088/1367-2630/12/4/043001 (2010).
43. Zwolak, M. & Vidal, G. Mixed-state dynamics in one-dimensional quantum lattice systems: A time-dependent superoperator renormalization algorithm. *Phys. Rev. Lett.* **93**, 207205, https://doi.org/10.1103/PhysRevLett.93.207205 (2004).
44. Verstraete, F., Garcia-Ripoll, J. J. & Cirac, J. I. Matrix product density operators: simulation of finite-temperature and dissipative systems. *Phys. Rev. Lett.* **93**, 207204, https://doi.org/10.1103/PhysRevLett.93.207204 (2004).
45. Schollwöck, U. The density-matrix renormalization group in the age of matrix product states. *Annals Phys.* **326**, 96, https://doi.org/10.1016/j.aop.2010.09.012 (2011).
46. Al-Assam, S., Clark, S. R., Jaksch, D. & TNT Development Team. Tensor Network Theory Library, Beta Version 1.2.0. Available at, http://www.tensornetworktheory.org (2016).
47. Al-Assam, S., Clark, S. R. & Jaksch, D. The Tensor Network Theory Library. *J. Stat. Mech.* **2017**, 093102, https://doi.org/10.1088/1742-5468/aa7df3 (2017).
48. Sciolla, B., Poletti, D. & Kollath, C. Two-time correlations probing the dynamics of dissipative many-body quantum systems: Aging and fast relaxation. *Phys. Rev. Lett.* **114**, 170401, https://doi.org/10.1103/PhysRevLett.114.170401 (2015).
49. Everest, B., Lesanovsky, I., Garrahan, J. P. & Levi, E. Role of interactions in a dissipative many-body localized system. *Phys. Rev. B* **95**, 024310, https://doi.org/10.1103/PhysRevB.95.024310 (2017).

50. He, L., Sieberer, L. M. & Diehl, S. Space-time vortex driven crossover and vortex turbulence phase transition in one-dimensional driven open condensates. *Phys. Rev. Lett.* **118**, 085301, https://doi.org/10.1103/PhysRevLett.118.085301 (2017).
51. Wang, R. R. W., Xing, B., Carlo, G. G. & Poletti, D. Period doubling in period-one steady states. *Phys. Rev. E* **97**, 020202, https://doi.org/10.1103/PhysRevE.97.020202 (2018).
52. Wolff, S., Bernier, J.-S., Poletti, D., Sheikhan, A. & Kollath, C. Evolution of two-time correlations in dissipative quantum spin systems: Aging and hierarchical dynamics. *Phys. Rev*. **100**, 165144, https://arxiv.org/abs/1809.10464v1 (2019).
53. Žnidarič, M. Exact solution for a diffusive nonequilibrium steady state of an open quantum chain. *J. Stat. Mech. Theor. Exp.* **2010**, L05002, https://doi.org/10.1088/1742-5468/2010/05/L05002 (2010).
54. Žnidarič, M. Solvable quantum nonequilibrium model exhibiting a phase transition and a matrix product representation. *Phys. Rev. E* **83**, 011108, https://doi.org/10.1103/PhysRevE.83.011108 (2011).
55. Capel, H. W. & Perk, J. H. H. Autocorrelation function of the *x*-component of the magnetization in the one-dimensional *XY* model. *Phys. A* **87A**, 211, https://doi.org/10.1016/0378-4371(77)90014-0 (1977).
56. Katsura, S., Horiguchi, T. & Suzuki, M. Dynamical properties of the isotropic XY model. *Physica* **46**, 67, https://doi.org/10.1016/0031-8914(70)90118-7 (1970).
57. Gómez-Ruiz, F. J., Mendoza-Arenas, J. J., Rodríguez, F. J., Tejedor, C. & Quiroga, L. Quantum phase transitions detected by a local probe using time correlations and violations of Leggett-Garg inequalities. *Phys. Rev. B* **93**, 035441, https://doi.org/10.1103/PhysRevB.93.035441 (2016).
58. Gómez-Ruiz, F. J., Mendoza-Arenas, J. J., Rodríguez, F. J., Tejedor, C. & Quiroga, L. Universal two-time correlations, out-of-time-ordered correlators, and Leggett-Garg inequality violation by edge Majorana fermion qubits. *Phys. Rev. B* **97**, 235134, https://doi.org/10.1103/PhysRevB.97.235134 (2018).
59. Robens, C., Alt, W., Meschede, D., Emary, C. & Alberti, A. Ideal Negative Measurements in Quantum Walks Disprove Theories Based on Classical Trajectories. *Phys. Rev. X* **5**, 011003, https://doi.org/10.1103/PhysRevX.5.011003 (2015).

Acknowledgements

J.J.M.-A. thanks Stephen Clark and Katarzyna Roszak for interesting discussions. We acknowledge financial support from Facultad de Ciencias-UniAndes- 2019 project Quantum thermalization and optimal control in many-body systems (Grant No. INV-2018-50-1384). We acknowledge financial support from Departamento Administrativo de Ciencia, Tecnología e Innovación Colciencias, through the project Producción y Caracterización de Nuevos Materiales Cuánticos de Baja Dimensionalidad: Criticalidad Cuántica y Transiciones de Fase Electrónicas (Grant No. 120480863414).

Author contributions

J.J. Mendoza-Arenas developed the theoretical framework and implemented the time evolution codes. F.J. Gómez-Ruiz developed numerical simulations and prepared the figures. All authors contributed to the analysis of the results and the writing of the manuscript. L. Quiroga and F.J. Rodríguez supervised the project.

Competing interests

The authors declare no competing interests.

Additional information

Supplementary information is available for this paper at https://doi.org/10.1038/s41598-019-54121-1.

Correspondence and requests for materials should be addressed to F.J.G.-R.

Reprints and permissions information is available at www.nature.com/reprints.

Publisher's note Springer Nature remains neutral with regard to jurisdictional claims in published maps and institutional affiliations.